

# Experimental study of velocity-scalar filtered joint density function for LES of turbulent combustion

Danhong Wang, Chenning Tong\*

*Department of Mechanical Engineering, Clemson University, Clemson, SC 29634-0921, USA*

---

## Abstract

The velocity-scalar filtered joint density function (FJDF) used in large eddy simulation (LES) of turbulent combustion is experimentally studied. Measurements are made in the fully developed region of an axisymmetric turbulent jet using an array consisting of three X-wires and resistance-wire temperature sensors. Filtering in the cross-stream and streamwise directions is realized by using the array and by invoking Taylor's hypothesis, respectively. The means of the FJDF conditional on the subgrid-scale (SGS) turbulent kinetic energy and the SGS scalar variance at a given location range from close to joint normal to bimodal with the peaks separated in both velocity and scalar spaces, which correspond to qualitatively different mixing regimes. For close to joint normal FJDFs, the SGS fields are well mixed. For bimodal FJDFs, the conditionally filtered scalar diffusion and dissipation strongly depend on the SGS velocity and scalar, consistent with a combination of diffusion layers and plane strain in the SGS fields, which is similar to the counter-flow model for laminar flamelets. The results suggest that in LES, both mixing regimes could potentially be modeled accurately. The velocity field affects the SGS variance and the filtered scalar dissipation rate primarily by changing the degree of nonequilibrium of the SGS scalar and the SGS time scale, respectively. This study further demonstrates the importance of including velocity in mixing models.

© 2004 The Combustion Institute. Published by Elsevier Inc. All rights reserved.

*Keywords:* Turbulent nonpremixed flames; Turbulent mixing; Large-eddy simulation

---

## 1. Introduction

Large-eddy simulation (LES) is gaining increasing importance as an approach for computing turbulent reacting flows. The scalar filtered density function (FDF) method [1] has been shown to be a highly effective way to account for the effects of the subgrid-scale (SGS) mixing. The method solves a FDF transport equation in which the effects of reactions on the evolution of the FDF are in closed form. However, it has the

limitation that the SGS transport must be modeled and that the SGS scalar mixing has to be modeled independent of the SGS velocity field.

A more advanced approach solves the velocity-scalar filtered joint density function (FJDF) transport equation in which scalar transport by the SGS velocity is also in closed form [2]. In addition, because molecular mixing is local in both composition and velocity spaces, inclusion of velocity information into mixing models can potentially result in more realistic descriptions of the SGS mixing. This approach has recently been established successfully [2]. To develop improved mixing models, an understanding of the physics of the SGS velocity and scalar fields is essential.

---

\* Corresponding author. Fax: +1 864 656 4435.

E-mail address: [ctong@ces.clemson.edu](mailto:ctong@ces.clemson.edu) (C. Tong).

Previous works have studied scalar FDF, velocity FJDF, and their transport equations [3–5]. In the present work, we investigate the velocity-scalar FJDF and its transport equation to further elucidate the fundamental physics of the SGS mixing, especially the influence of the velocity field.

The velocity-scalar FJDF,  $f_{u\phi}(\mathbf{v}, \hat{\phi}; \mathbf{x}, t)$ , is defined as [6,7,2]

$$\int \prod_{i=1}^3 \delta[u_i(\mathbf{x}', t) - v_i] \delta[\phi(\mathbf{x}', t) - \hat{\phi}] G(\mathbf{x}' - \mathbf{x}) d\mathbf{x}' \\ = \left\langle \prod_{i=1}^3 \delta(u_i - v_i) \delta(\phi - \hat{\phi}) \right\rangle_L, \quad (1)$$

where  $\mathbf{v}$  and  $\hat{\phi}$  are the sample-space variables for the fluid velocity  $\mathbf{u}$  and the scalar  $\phi$ ;  $\delta$  and  $G$  are the Dirac delta function and the filter function, respectively. The integration is over all physical space. Filtered and ensemble-averaged variables are denoted as  $\langle \cdot \rangle_L$  and  $\langle \cdot \rangle$ , respectively.

The transport equation of the FJDF can be obtained using a method by Pope [8,2]:

$$\frac{\partial f_{u\phi}}{\partial t} + v_j \frac{\partial f_{u\phi}}{\partial x_j} = \frac{\partial \langle p \rangle_L}{\partial x_j} \frac{\partial f_{u\phi}}{\partial v_j} \\ + \frac{\partial}{\partial v_j} \left\{ \left\langle \frac{\partial p''}{\partial x_j} \middle| \mathbf{u} = \mathbf{v}, \phi = \hat{\phi} \right\rangle_L f_{u\phi} \right\} \\ - \frac{\partial}{\partial v_i} \left\{ \left\langle v \frac{\partial^2 u_i}{\partial x_j \partial x_j} \middle| \mathbf{u} = \mathbf{v}, \phi = \hat{\phi} \right\rangle_L f_{u\phi} \right\} \\ - \frac{\partial}{\partial \hat{\phi}} \left\{ \left\langle D \frac{\partial^2 \phi}{\partial x_j \partial x_j} \middle| \mathbf{u} = \mathbf{v}, \phi = \hat{\phi} \right\rangle_L f_{u\phi} \right\}, \quad (2)$$

where  $\nu$  and  $D$  are the molecular viscosity and diffusivity, respectively, and  $\langle \cdot | \mathbf{u} = \mathbf{v}, \phi = \hat{\phi} \rangle_L$  denotes a conditionally filtered variable. The left-hand side of Eq. (2) is the time rate of change and advection in physical space. The first three terms on the right-hand side represent transport in velocity space by the resolvable-scale pressure gradient, by the SGS pressure gradient, and by viscous acceleration. The fourth term is transport in scalar space by molecular diffusion. The alternatives to the viscous acceleration and molecular diffusion are the conditionally filtered velocity dissipation tensor,  $\langle \epsilon_{ik} | \mathbf{u} = \mathbf{v}, \phi = \hat{\phi} \rangle_L$ , and scalar dissipation,  $\langle \chi | \mathbf{u} = \mathbf{v}, \phi = \hat{\phi} \rangle_L$ , where  $\epsilon_{ik} = \nu \frac{\partial u_i}{\partial x_j} \frac{\partial u_k}{\partial x_j}$  and  $\chi = D \frac{\partial \phi}{\partial x_j} \frac{\partial \phi}{\partial x_j}$  are the dissipation rate tensor and the scalar dissipation rate, respectively. Galilean invariance of the velocity FJDF and its transport equation has been shown [9]. Gicquel et al. [10] developed a stochastic model based on the Generalized Langevin Model developed for the PDF method. Sheikhi et al. [2] recently have developed a velocity-scalar FJDF method, and the results using the FJDF are in good agreement with DNS results.

In the present work, we study the velocity-scalar FJDF and several of the SGS terms in the

FJDF equation. Unlike PDFs, a FJDF is not a statistic, but a random process and must be characterized statistically. For a filter size smaller than the integral length scales, the mean FJDF approximately equals the velocity-scalar JPDF, which is generally not far from joint-Gaussian in regions of fully developed flows without large-scale intermittency [11].

Other important characteristics of the FJDF can be revealed by its conditional means. Previous investigations of conditional scalar FDF, scalar-scalar dissipation FJDF, and velocity FJDF have shown that the SGS scalar and velocity at a given location are on average in equilibrium and non-equilibrium for small and large instantaneous SGS variance (or energy), respectively [3–5]. The SGS scalar variance is defined as  $\langle \phi''^2 \rangle_L = \int [\phi(\mathbf{x}') - \langle \phi \rangle_L(\mathbf{x})]^2 G(\mathbf{x}' - \mathbf{x}) d\mathbf{x}'$ . (The mean SGS variance,  $\langle \langle \phi''^2 \rangle_L \rangle$ , is denoted as  $\langle \phi''^2 \rangle$ ). The SGS energy  $k_L$  is defined as  $\frac{1}{2} (\langle u''^2 \rangle_L + \langle v''^2 \rangle_L)$ . Both are fluctuating variables and have approximately log-normal PDFs [3,12]. Here for convenience we refer to both the cases of the SGS production equal to and smaller than the dissipation as quasi-equilibrium because the conditional SGS fields have very similar characteristics. For equilibrium SGS scalar, the FDF is on average close to Gaussian, and the scalar dissipation has only moderate dependence on the SGS scalar. However, for nonequilibrium SGS scalar, the FDF is bimodal and the scalar dissipation strongly depends on the SGS scalar. The SGS scalar is also characterized by the existence of diffusion-layer-like structure (ramp-cliffs). These characteristics are similar to those of the scalar PDF in the early stages of initially binary mixing [13]. For equilibrium SGS velocity, the velocity FJDF is close to joint normal. For nonequilibrium SGS velocity, the FJDF has a uniform region, which has not been previously observed, suggesting that the SGS velocity is undergoing local rapid distortion [5].

Previous studies of the velocity-scalar JPDF equation have shown that in a fully developed flow the scalar diffusion has a linear dependence on the scalar and velocity fluctuations [14]. However, when conditioned on the velocity alone the dependence becomes weaker as the high Reynolds number increases [15]. Previous results for the scalar and velocity FDFs suggest that the velocity-scalar FJDF will also have qualitatively different characteristics for equilibrium and non-equilibrium SGS velocity and scalar. Because the conditional FDFs for the equilibrium and non-equilibrium regimes are dominated by different structures and dynamics, they can potentially be modeled more accurately than the unconditioned FDF (or PDF), leading to improved LES statistics. In this work, we use experimental data obtained in the fully developed region of an axisymmetric turbulent jet to analyze the velocity-scalar FJDF and its transport equation.

## 2. Experimental facilities

The jet facility was housed in a large, air-conditioned room. The jet assembly was mounted vertically. A collection hood at a downstream distance of 260 nozzle diameters (3.9 m) minimizes the effects of the ceiling on the jet. Jet air supply was heated with a pipe heater before entering the plenum chamber, producing an excess temperature (above the ambient) of 20 °C at the nozzle exit.

Measurements were made for a jet exit velocity  $U_j$  of 40 m/s, which gives a jet Reynolds number  $Re_j$  of 40,000. The nozzle diameter  $D_j$  was 15 mm. Refer to Table 1 for other flow parameters. Data were collected at a downstream distance of  $x/D_j = 80$  on the jet centerline. The effects of the initial jet-to-air density ratio ( $\approx 0.93$ ) on the properties of the jet, such as the spreading rate and the RMS fluctuations of velocity and temperature, were small [16]. Thus, in our measurements the temperature fluctuations were dynamically passive.

Measurements of the FJDF require spatial filtering of turbulent velocity and scalar fields. Due to the difficulties in obtaining three-dimensional data experimentally, two-dimensional (streamwise and radial directions) filtering was employed. In the present study, the streamwise filtering was performed by invoking Taylor’s hypothesis, and the cross-stream filtering was realized with three hot-wire and resistance-wire sensors aligned in the cross-stream direction (Fig. 1). To minimize the error associated with invoking Taylor’s hypothesis, instantaneous convection velocity obtained by low-pass filtering the streamwise velocity component with a larger filter was used.

The array filter technique was proposed and studied by Tong et al. [17], and has been used by a number of authors to study the SGS stress [18] and conditional FDF [3]. In this (and previous [3,4,19]) studies, we use box filters because a scalar FDF obtained with a box filter is easily interpreted. Our estimates using a spectral model for inertial-range isotropic turbulence show that the array filter overestimates the mean SGS energy and SGS scalar variance by 13%. The mean SGS velocity variance  $\langle u_1'^2 \rangle$  and  $\langle u_2'^2 \rangle$  (double primes denote an SGS variable) are overestimated by 16% and 10%, respectively. These errors are not negligible but are not expected to have significant effects on the measured FJDF, since much larger changes in  $k_L$  and  $\langle \phi''^2 \rangle_L$  are needed to alter the shape of the conditional FJDF (see Section 3).

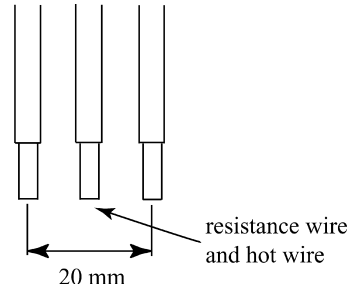


Fig. 1. A magnified view of the sensor array.

Therefore, we expect that the box-array filter will produce FJDF statistics similar to those using a true two-dimensional box filter.

In the present study, three filter widths, 10, 20, and 40 mm, were used. These correspond to  $\Delta/\ell = 0.13, 0.27, 0.53$  and  $\Delta/\eta = 63, 125, 250$ , respectively. Here,  $\eta$  ( $= 0.16$  mm) is the Kolmogorov scale. The scalar dissipation scale  $\eta_\phi$  is 0.22 mm. The integral length scale  $\ell$  is estimated as 75 mm using  $\langle u_1'^2 \rangle^{3/2} / \langle \epsilon \rangle$ , where  $\epsilon$  is computed as  $5\nu\{(\partial u_1/\partial x_1)^2 + (\partial u_2/\partial x_1)^2\}$ . These filter sizes were chosen to be much larger than the dissipation scales because in LES of high-Reynolds-number flows the grid size is generally in the inertial range (close to the integral length scales). Our previous results [3] have shown that as the filter scale decreased to approximately 30–40 Kolmogorov scales, the results began to show characteristics of those obtained with a dissipation-scale filter, therefore were not representative of the situation of LES in high-Reynolds-number flows. The SGS variances are given in Table 2. The spectra of the streamwise velocity and resolvable-scale velocity are given in [5].

Temperature fluctuations were measured with platinum resistance wires. Details of the devices are given in [19]. Velocity measurements were made with three X-wire probes operated by TSI IFA 100 hot-wire anemometers with an overheat ratio of 1.8. The probes were calibrated using a

Table 2  
SGS variances on the jet centerline at  $x/D_j = 80$

$\Delta/\eta$ ( $\Delta/\ell$ )	$\langle u_1'^2 \rangle$	$\langle u_2'^2 \rangle$ (m <sup>2</sup> /s <sup>2</sup> )	$\langle \phi''^2 \rangle / \langle \phi^2 \rangle$
63 (0.13)	0.107	0.089	0.189
125 (0.27)	0.174	0.140	0.317
250 (0.53)	0.261	0.205	0.462

Table 1  
Jet parameters on the centerline at  $x/D_j = 80$

$\langle U \rangle$	$\langle u_1'^2 \rangle^{1/2}$	$\langle u_2'^2 \rangle^{1/2}$	$R_\lambda$	$\epsilon$	$\eta$	$\eta_\phi$	$\ell$
3.07 m/s	0.72 m/s	0.61 m/s	229	5.25 m <sup>2</sup> /s <sup>3</sup>	0.16 mm	0.22 mm	75 mm

modification of a method by Browne et al. [20,5]. Due to the high signal-to-noise ratio of the resistance-wire temperature device, a very low excess temperature (1.25 °C at the measurement location) can be used, rendering the temperature contamination of hot wires negligible. For the statistics considered, the differences between the corrected and uncorrected results are within 2%. Therefore, the uncorrected results are given.

The velocity and temperature signals were low-pass filtered at 5 kHz and amplified by Krohn-Hite 3364 filter/amplifiers. The signals were digitized at 10 k samples/second by a 12-bit National Instrument A/D converter (PCI-6071E) which has a maximum sampling rate of  $1.25 \times 10^6$  samples/second so that the inter-channel delay is much shorter than the sample interval. In the present study, most of the statistics computed are conditional statistics with two to four conditioning variables. We achieve sufficient statistical convergence by monitoring the results when the sample size is increased. We find that  $2 \times 10^8$  data samples are needed.

### 3. Results and discussions

In this section, the results of the measured conditional FJDF are presented. Only results for  $\Delta/\eta = 125$  are shown. The results for  $\Delta/\eta = 63$  and  $\Delta/\eta = 250$  are qualitatively similar.

#### 3.1. The conditional FJDF

The mean FJDF conditional on the resolvable-scale velocity, the resolvable-scale scalar, the SGS energy, and the SGS scalar variance,  $\langle f_{u\phi} | \langle \mathbf{u} \rangle_L, \langle \phi \rangle_L, k_L, \langle \phi''^2 \rangle_L$  measured on the jet centerline is shown in Fig. 2. The FJDF is normalized by  $(2k_L)^{1/2}$  and  $\langle \phi''^2 \rangle_L^{1/2}$ . Note that for a specified value of the resolvable-scale velocity, the SGS velocity is equivalent to the total velocity. Similarly the SGS scalar is equivalent to the total scalar for a specified value of the resolvable-scale scalar. For convenience, we use  $u'_i$  and  $\phi''$ , and omit the sam-

ple-space variables  $v_i$  and  $\hat{\phi}$  when plotting the FJDF and other conditionally filtered variables. We present results for different  $\langle \phi''^2 \rangle_L$  and  $k_L$  values but fixed  $\langle \mathbf{u} \rangle_L (= \langle \mathbf{u} \rangle)$  and  $\langle \phi \rangle_L (= \langle \phi \rangle)$  because the FJDF has a strong dependence on  $\langle \phi''^2 \rangle_L$  and  $k_L$  but is relatively insensitive to  $\langle \mathbf{u} \rangle_L$  and  $\langle \phi \rangle_L$ . For small  $\langle \phi''^2 \rangle_L (0.69 \langle \phi''^2 \rangle)$  and  $k_L (0.57 \langle k_L \rangle)$ , the conditional FJDF of  $u_1$  and  $\phi$  is close-to-joint-Gaussian (Fig. 2A), consistent with the close-to-Gaussian marginal FDFs previously observed [3,5] (the results for  $u_2$  and  $\phi$  are similar). The SGS velocity and scalar are essentially uncorrelated with the correlation coefficient  $\rho_{u'_1 \phi''} = \langle \frac{u'_1 \phi''}{(k_L \langle \phi''^2 \rangle_L)^{1/2}} | k_L, \langle \phi''^2 \rangle_L \rangle = 0.028$ . The velocity-scalar JPFD measured at the same location is also close to joint normal [11] (except that the velocity and scalar are correlated). Because a fully developed jet is in quasi-equilibrium, the similarity between the FJDF and the JPFD suggests that the SGS velocity and scalar are also in quasi-equilibrium when the SGS energy and the SGS variance are small.

For large  $k_L (3.1 \langle k_L \rangle)$  and small  $\langle \phi''^2 \rangle_L$ , the FJDF (not shown) is also unimodal but may be somewhat flatter in the  $u'_1$  direction, since the  $u_1 - u_2$  FJDF has a uniform region [5]. The correlation between  $u'_1$  and  $\phi''$  is higher than that for small  $k_L$  but is still low ( $\rho_{u'_1 \phi''} = 0.13$ ). The correlation between  $u'_2$  and  $\phi''$  is zero due to symmetry of the flow). Previous studies [12,5] have shown that the SGS turbulence is under local rapid distortion when the SGS energy is large. However, for small SGS variance, the SGS scalar is well mixed, indicating that the rapid distortion does not produce much larger SGS correlation or alter the scalar FDF.

For large  $\langle \phi''^2 \rangle_L (4.5 \langle \phi''^2 \rangle)$  the FJDF is bimodal regardless of the values of  $k_L$  (Figs. 2B and C). For small  $k_L$ , the peaks of the FJDF are close to  $\phi'' / \langle \phi''^2 \rangle_L^{1/2} \approx \pm 1$  and not far from  $u'_1 = 0$ . The correlation between  $u'_1$  and  $\phi''$  is somewhat higher ( $\rho_{u'_1 \phi''} = 0.23$ ), indicating a moderate SGS scalar flux. For large  $k_L$  the correlation is much stronger ( $\rho_{u'_1 \phi''} = 0.52$ ) and the two peaks of the FJDF are separated in both the velocity and scalar spaces.

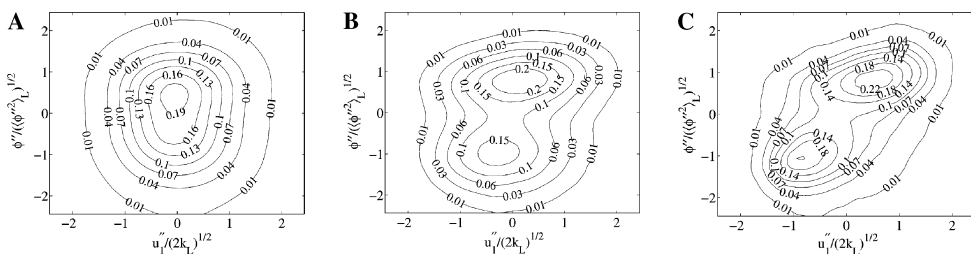


Fig. 2. Conditional mean of the FJDF on the jet centerline for  $\langle u_1 \rangle_L = \langle u_1 \rangle$ ,  $\langle u_2 \rangle_L = 0$ , and  $\langle \phi \rangle_L = \langle \phi \rangle$ . ( $\Delta/\eta = 125$  for all figures.) (A)  $k_L/\langle k_L \rangle = 0.57$ ,  $\langle \phi''^2 \rangle_L/\langle \phi''^2 \rangle = 0.69$ ; (B)  $k_L/\langle k_L \rangle = 0.57$ ,  $\langle \phi''^2 \rangle_L/\langle \phi''^2 \rangle = 4.5$ ; and (C)  $k_L/\langle k_L \rangle = 3.13$ ,  $\langle \phi''^2 \rangle_L/\langle \phi''^2 \rangle = 4.5$ .

There is a “neck” near  $u_1'' = 0$  and  $\phi'' = 0$ , therefore the SGS scalar mixing is expected to be most intense near this point. This FJDF shape is consistent with a scalar diffusion layer associated with a local plane strain (converging–diverging) velocity field. In such a structure, the scalar gradient is the largest in the diffusion layer where the SGS velocity parallel to the compressive eigenvector of the strain rate tensor (and to the normal vector of the layer) is small, similar to the counter-flow model for laminar flamelets [21]. In the jet, the normal vector of a diffusion layer is preferentially oriented and is generally within  $45^\circ$  from the streamwise direction; therefore,  $u_1''$  is on average small in the layer, and the FJDF peaks are separated in  $u_1''$  space (the FJDF of  $u_2$  and  $\phi$  is symmetric about  $u_2'' = 0$  due to flow symmetry). By contrast, the peaks of the FJDF in Fig. 2B overlap in the velocity space; thus, mixing can occur over a wide range of SGS velocity, and its dependence on the SGS velocity is weaker. Because under such conditions the scalar FDF is bimodal, it is likely that there still exist diffusion layers (cliffs) with large scalar value jumps. Such a SGS scalar structure could result from local rapid distortion at scales smaller than the filter scale.

The above results also show that the correlation between the SGS velocity and scalar is weak for small SGS scalar variance and SGS kinetic energy but increases with these variables. In Fig. 3,

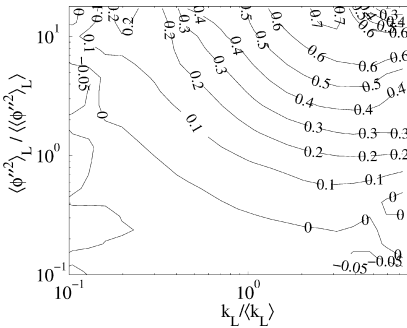


Fig. 3. Conditional correlation between  $u_1''$  and  $\phi''$ .

we plot their conditional correlation coefficient, which generally increases faster with  $\langle \phi''^2 \rangle_L$  than with  $k_L$ . For small  $\langle \phi''^2 \rangle_L (< 1)$ , the correlation remains less than 0.2 even for large SGS energy. For large  $\langle \phi''^2 \rangle_L$ , the dependence on  $k_L$  is stronger. For  $\langle \phi''^2 \rangle_L / \langle \phi''^2 \rangle_L > 10$  and  $k_L / \langle k_L \rangle > 2$ ,  $\rho$  is as high as 0.7 due to the combination of the linear SGS velocity structure and the diffusion layers in the SGS scalar.

The high correlation is also associated with nonequilibrium SGS scalar. The normalized conditional production rate of the SGS scalar variance (two components),  $P_{\phi L} / \chi_L = -(\langle \phi u_i \rangle_L - \langle \phi \rangle_L \langle u_i \rangle_L) (\partial \phi) / (\partial x_i) / \chi_L$ ,  $i = 1$  and 2 (not shown), which is a measure of the degree of nonequilibrium of the SGS scalar, increases with both  $\langle \phi''^2 \rangle_L$  and  $k_L$ , and the isocontours are similar to those of the conditional correlation. The results suggest that a nonequilibrium SGS scalar requires large SGS variance but only moderate SGS energy.

### 3.2. The conditionally filtered scalar diffusion and dissipation

The conditionally filtered scalar diffusion and dissipation are unclosed terms in the FJDF equation. In this study, they are obtained using streamwise derivatives. For small  $\langle \phi''^2 \rangle_L$ , the conditionally filtered diffusion (one component)  $D \langle \partial^2 \phi / \partial x_1^2 | \mathbf{u}'', \phi'' \rangle_L$  has approximately equally spaced straight-line isocontours, thereby having a linear dependence on both  $u_1''$  and  $\phi''$ . For small  $k_L$  and  $\langle \phi''^2 \rangle_L$ , the dependence on the SGS velocity is weak (Fig. 4A). For large  $k_L$ , the isocontours (not shown) have larger slopes and a somewhat stronger dependence on  $u_1''$ . The linear dependence is similar to the results for the conditional diffusion  $D \langle \nabla^2 \phi | \mathbf{u}, \phi \rangle$  in the velocity-scalar JPFD equation. It is also consistent with a previous linear model [14] in which the dependence of  $D \langle \nabla^2 \phi | \mathbf{u}, \phi \rangle$  on  $\mathbf{u}$  for joint normal velocity-scalar fields is stronger for higher  $u - \phi$  and  $\nabla u - \nabla \phi$  correlations. Since the  $\nabla u - \nabla \phi$  correlation generally decreases with increasing Reynolds number due to local isotropy, the model predicts that the diffusion conditional on the velocity alone  $D \langle \nabla^2 \phi | \mathbf{u} \rangle$  vanishes at high Reynolds numbers [14]. The dependence of  $D \langle \partial^2 \phi / \partial x_1^2 | \mathbf{u}'', \phi'' \rangle_L$  on the SGS

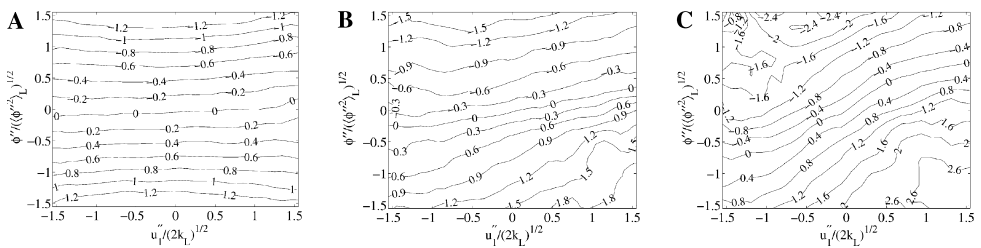


Fig. 4. Conditionally filtered scalar diffusion  $D \langle \frac{\partial^2 \phi}{\partial x_1^2} | u_1'', \phi'' \rangle_L | \langle u_1 \rangle_L, k_L, \langle \phi \rangle_L, \langle \phi''^2 \rangle_L$ . Conditions same as in Fig. 2.

velocity is also expected to increase with the  $u'' - \phi''$  correlation and to decrease with increasing Reynolds number based on the filter scale  $Re_\Delta = (\frac{1}{2}k_L)^{1/2} \Delta/v$ . Therefore, the stronger dependence of the diffusion for larger  $k_L$  is due to the higher  $u'' - \phi''$  correlation (0.13) than that for Fig. 4A (0.028).

For large  $\langle \phi''^2 \rangle_L$ , the dependence of the conditionally filtered diffusion on  $\phi''$  is nonlinear and the surface plot (not shown) has an S-shape. Figure 4B shows the isocontours for the diffusion for large  $\langle \phi''^2 \rangle_L$  (6.09 $\langle \phi''^2 \rangle$ ) but small  $k_L$ . The isocontours are more closely spaced near  $\phi'' = 0$ , suggesting that in addition to an approximately linear trend, an S-shaped dependence on  $\phi''$  exists for all  $u''_1$  values. This is consistent with the FJDF in Fig. 2B, which shows that the bimodal scalar distribution spans over a wide range of velocity. The conditional diffusion  $D(\nabla^2 \phi | \phi)$  also has an S-shaped dependence on  $\phi$  in the early stages of initially binary mixing [22]. For large SGS energy,  $D(\partial^2 \phi / \partial x_1^2 | u'', \phi'')_L$  depends more strongly on  $u''_1$ , consistent with the stronger dependence of the FJDF on  $u''_1$  (Fig. 2C). In addition, the isocontours are closely spaced near  $u''_1 = 0$  and  $\phi'' = 0$ , suggesting that the most intense mixing occurs at small SGS velocity.

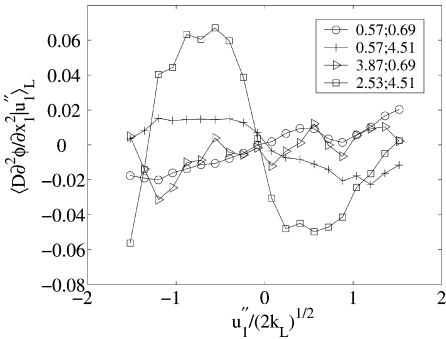


Fig. 5. Conditionally filtered scalar diffusion conditional on the SGS velocity  $\langle D(\partial^2 \phi / \partial x_1^2 | u''_1)_L | (u_1)_L, k_L, \langle \phi \rangle_L, \langle \phi''^2 \rangle_L$ . The values of  $k_L$  and  $\langle \phi''^2 \rangle_L$  are given in the legend.

The conditionally filtered diffusion conditional on the SGS velocity alone,  $D(\partial^2 \phi / \partial x_1^2 | u''_1)_L$  (Fig. 5) shows a significant dependence on  $u''_1$  when both  $\langle \phi''^2 \rangle_L$  and  $k_L$  are large whereas for other values the dependence is much weaker. Because the existence of diffusion layers and local plane strain is Reynolds number independent, the dependence of  $D(\partial^2 \phi / \partial x_1^2 | u''_1)_L$  on  $u''_1$  at large SGS variance and SGS energy is likely to persist even at high Reynolds numbers.

The conditionally filtered scalar dissipation (one component),  $\langle \chi_1 | u'', \phi'' \rangle_L$  [here  $\chi_1 = D(\partial \phi / \partial x_1)^2$ ], provides an alternative to  $D(\partial^2 \phi / \partial x_1^2 | u''_1, \phi''_1)_L$ . For small  $\langle \phi''^2 \rangle_L$ , the conditional mean of  $\langle \chi_1 | u''_1, \phi'' \rangle_L$  has a moderate dependence on the velocity and scalar, respectively (Fig. 6A). The correspondence between this result and the approximately joint normal FJDF in Fig. 2A is consistent with the previous findings that a constant conditional dissipation generally corresponds to a Gaussian PDF [22], further indicating that the SGS scalar is well mixed. For small  $k_L$  and large  $\langle \phi''^2 \rangle_L$ , the dissipation (Fig. 6B) has a bell-shaped dependence on  $\phi''$  but only a weak dependence on  $u''_1$ . This dependence on  $\phi''$  is consistent with the bimodal FJDF in Fig. 2B and the S-shaped diffusion plot in Fig. 4B.

For large  $k_L$  and  $\langle \phi''^2 \rangle_L$ , the dissipation has a peak at  $\phi'' = 0$  and  $u''_1 = 0$  (Fig. 6C), and decreases as the magnitude of  $u''_1$  increases, indicating a strong influence of the SGS velocity on the SGS mixing. The location of the peak dissipation corresponds to the “neck” region of the FJDF in Fig. 2C. This is consistent with the notion that the diffusion layer is associated with a converging-diverging (e.g., plane strain) velocity field. In such a structure, the velocity component normal to the diffusion layer is small near the layer center. Since diffusion layers have been shown to exist at very high Reynolds numbers, the observed dependence of scalar diffusion and dissipation on the velocity is likely to persist at high Reynolds numbers.

The above results show that when the SGS variance is large there is strong statistical dependence between scalar mixing (dissipation-scale scalar) and the SGS velocity field. The SGS scalar and velocity structures (especially when the SGS energy is also large) are similar to the structure of

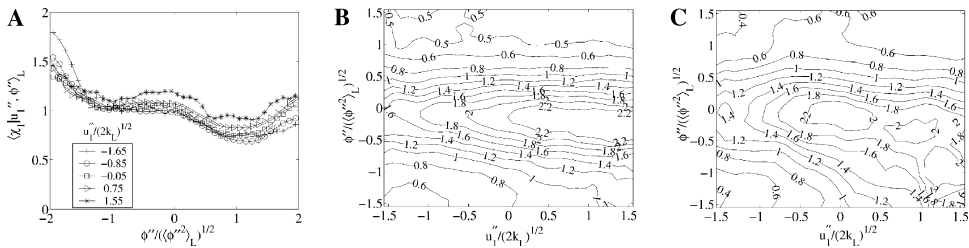


Fig. 6. Conditionally filtered scalar dissipation  $\langle \chi_1 | u''_1, \phi'' \rangle_L | (u_1)_L, k_L, \langle \phi \rangle_L, \langle \phi''^2 \rangle_L$ . Conditions same as in Fig. 2.

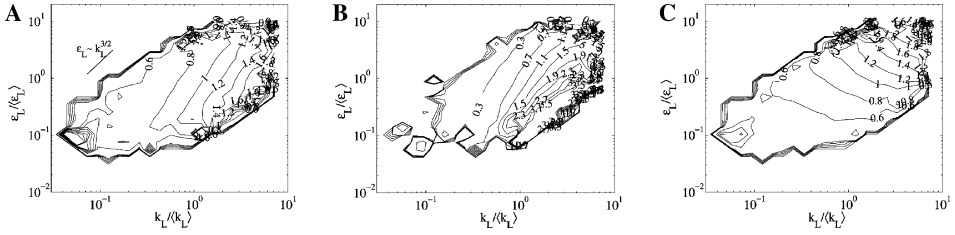


Fig. 7. Conditional SGS scalar variance (A), SGS variance production (B), and filtered dissipation (C) conditional on  $\epsilon_L$  and  $k_L$ .

laminar flamelets, thus the ability of mixing models to reflect such a structure is important for ensuring the localness of mixing (e.g., no mixing of fluid particles on the opposite sides of a flamelet). The results further demonstrate the importance of the velocity in mixing and of including velocity in mixing models.

3.3. The dependence of  $\langle \phi''^2 \rangle_L$  and  $\chi_{1L}$  on the SGS velocity

The SGS scalar variance and the filtered scalar dissipation rate,  $\chi_L \equiv \langle \chi \rangle_L$ , are important variables determining the shape of the scalar FDF [3,19]. In addition, at the level of velocity-scalar FJDF,  $\chi_L$  is needed to model molecular mixing [2]. It is therefore of importance to examine the influence of the velocity field on these variables.

The conditional mean of  $\langle \phi''^2 \rangle_L$  conditional on the filtered energy dissipation  $\epsilon_L \equiv \langle \epsilon \rangle_L$  and the SGS energy,  $\langle \langle \phi''^2 \rangle_L | \epsilon_L, k_L \rangle$ , is given in Fig. 7A. The results with sufficient statistical convergence are limited to an elliptic region that approximately corresponds to the isocontours of the  $\epsilon_L - k_L$  JPFD [5]. At  $\epsilon_L / \langle \epsilon \rangle = 1$  and  $k_L / \langle k_L \rangle = 1$ , the SGS variance is close to its mean value  $\langle \langle \phi''^2 \rangle_L | \epsilon_L, k_L \rangle = 0.9 \langle \phi''^2 \rangle$ , indicating that the SGS scalar is close to its average conditions. Toward the lower right portion of the  $\epsilon_L - k_L$  plane, the SGS variance increases.

To understand this trend, we compute the conditional means of the SGS variance production,  $\langle P_{\phi L} | \epsilon_L, k_L \rangle$ . The result given in Fig. 7B is normalized by  $\langle \chi_{1L} | \epsilon_L, k_L \rangle$ , therefore represents the balance between the production and dissipation, i.e., the degree of nonequilibrium of the SGS scalar. Similar to the SGS variance, the production also increases toward the lower right portion of the  $\epsilon_L - k_L$  plane. In addition, the isocontours have approximately the same slopes as those of  $\langle \langle \phi''^2 \rangle_L | \epsilon_L, k_L \rangle$ , suggesting that  $\langle \langle \phi''^2 \rangle_L | \epsilon_L, k_L \rangle$  is largely determined by the degree of nonequilibrium of the SGS scalar and increases with it.

The conditionally filtered scalar dissipation rate,  $\langle \chi_{1L} | \epsilon_L, k_L \rangle$ , has isocontours approximately perpendicular to those of  $\langle \langle \phi''^2 \rangle_L | \epsilon_L, k_L \rangle$  (Fig. 7C), i.e.,  $\chi_{1L}$  changes the fastest when the degree of nonequilibrium of the SGS scalar is held con-

stant (along the isocontours of  $\langle \langle \phi''^2 \rangle_L | \epsilon_L, k_L \rangle$  and  $\langle P_{\phi L} | \epsilon_L, k_L \rangle$ ). For quasi-equilibrium spectral transfer, the filtered dissipation scales as  $\chi_L \sim \langle \phi''^2 \rangle_L / \tau_{\phi L}$ , where  $\tau_{\phi L}$  is the SGS scalar time scale. Therefore, Fig. 7C suggests that the increase of  $\chi_{1L}$  along the isocontours of  $\langle \phi''^2 \rangle_L$  is due to the decrease in  $\tau_{\phi L}$  caused by the velocity field. The results in Figs. 7B and C suggest that the SGS velocity causes  $\chi_{1L}$  and  $\langle \phi''^2 \rangle_L$  to increase by decreasing the SGS scalar time scale and by increasing the degree of nonequilibrium of the SGS scalar, respectively.

To further examine the effects of the velocity field, we consider its equilibrium property. A measure of the degree of nonequilibrium of the SGS velocity is the conditional production of the SGS energy  $\langle P_L | k_L, \epsilon_L \rangle | \epsilon_L$ , where  $P_L = -\langle u_i u_i \rangle_L - \langle u_i \rangle_L \langle u_i \rangle_L \partial u_i / \partial x_i$ ,  $i = 1$  and 2. Its isocontours (not shown) in the region  $k_L > \langle k_L \rangle$  have slopes similar to those of  $\langle P_{\phi L} | k_L, \epsilon_L \rangle / \chi_{1L}$ , suggesting that the observed trends for  $\langle \langle \phi''^2 \rangle_L | \epsilon_L, k_L \rangle$  and  $\langle \chi_{1L} | \epsilon_L, k_L \rangle$  are largely related to the degree of nonequilibrium and the time scale of the SGS velocity. Therefore, the velocity affects  $\langle \langle \phi''^2 \rangle_L | \epsilon_L, k_L \rangle$  and  $\langle \chi_{1L} | \epsilon_L, k_L \rangle$  through different processes which appear to have “orthogonal” effects.

These results have implications for SGS modeling. The filtered scalar dissipation has been modeled by assuming local equilibrium  $\chi_L = P_{\phi L}$  [23]. Figure 7B suggests that the model can be improved by including  $\epsilon_L$  and  $k_L$  to account for the departure from equilibrium spectral transfer. The production  $P_{\phi L}$  is available in velocity-scalar FJDF calculations and can be used to model  $\chi_L$ . In addition, for LES that solves scalar transport equations  $P_{\phi L} / \chi_L$  can be modeled using  $\langle \langle \phi''^2 \rangle_L | \epsilon_L, k_L \rangle$  and a scalar time scale determined by  $\epsilon_L$  and  $k_L$ . The results for  $\langle \langle \phi''^2 \rangle_L | \epsilon_L, k_L \rangle$  can also be used to test models for  $\langle \phi''^2 \rangle_L$ .

4. Conclusions

The velocity-scalar FJDF and its transport equation are studied. Qualitatively different results are obtained for small and large values of  $\langle \phi''^2 \rangle_L$  and  $k_L$ .

The conditional FJDF generally is not far from joint Gaussian for small values of  $\langle \phi''^2 \rangle_L$  and  $k_L$ . The correlation between the SGS velocity and scalar is weak, i.e., the SGS scalar flux is small. The conditionally filtered scalar diffusion has a linear dependence on both  $\phi''$  and  $u_1''$ , and the conditionally filtered scalar dissipation has a moderate dependence on these variables, indicating well-mixed SGS fields. For small  $\langle \phi''^2 \rangle_L$  but large  $k_L$ , the results remain qualitatively similar, indicating that the local rapid distortion under this condition does not significantly alter the SGS scalar field.

For large  $\langle \phi''^2 \rangle_L$ , the FJDF is bimodal. For small  $k_L$ , the peaks (dominant scalar values) overlap in the velocity space. The scalar diffusion and dissipation have S-shaped and bell-shaped dependence on  $\phi''$ , respectively. Their dependences on  $u_1''$  are moderate. Therefore, intense SGS mixing occurs over a range of SGS velocities. For large  $k_L$  the peaks are separated in the velocity space, suggesting that the SGS fields contain a combination of diffusion layers and plane strain. Both the diffusion and dissipation depend strongly on the  $\phi''$  and  $u_1''$ . The most intense mixing occurs in the center region of the diffusion layers where the SGS velocity is small. Therefore, the SGS mixing and its dependence on the SGS velocity are qualitatively different for different ranges of  $\langle \phi''^2 \rangle_L$  and  $k_L$  values, and it is important for mixing models to correctly predict these mixing regimes. The results also suggest that when both  $k_L$  and  $\langle \phi''^2 \rangle_L$  are large the conditionally filtered diffusion conditional on the velocity  $D(\nabla^2 \phi | \mathbf{u}'')_L$  might not vanish at high Reynolds numbers.

We also examine the effects of the velocity on the SGS variance and the filtered scalar dissipation rate. We find that the velocity field affects  $\langle \phi''^2 \rangle_L$  and  $\chi_{1L}$  primarily by changing the degree of nonequilibrium of the SGS scalar and the SGS time scale, respectively. The results can be used to improve models for  $\langle \phi''^2 \rangle_L$  and  $\chi_L$ .

### Acknowledgments

The support of AFOSR under Grant No. F-49620-02-1-0130 (Dr. Julian M. Tishkoff, program

manager) is gratefully acknowledged. We thank Professor Stephen B. Pope for reading the draft paper and providing valuable comments.

### References

- [1] P.J. Colucci, F.A. Jaber, P. Givi, S.B. Pope, *Phys. Fluids* 10 (1998) 499–515.
- [2] M.R.H. Sheikhi, T.G. Drozda, P. Givi, S.B. Pope, *Phys. Fluids* 15 (2003) 2321–2337.
- [3] C. Tong, *Phys. Fluids* 13 (2001) 2923–2937.
- [4] D. Wang, C. Tong, *Phys. Fluids* 14 (2002) 2170–2185.
- [5] D. Wang, C. Tong, S.B. Pope, *Phys. Fluids* 16 (2004) 3599–3613.
- [6] S.B. Pope, *Proc. Combust. Inst.* 23 (1990) 591–612.
- [7] F. Gao, E.E. O'Brien, *Phys. Fluids A* 5 (1993) 1282–1284.
- [8] S.B. Pope, *Prog. Eng. Combust. Sci.* 11 (1985) 119–192.
- [9] C. Tong, *Phys. Fluids* 15 (2003) 2073–2076.
- [10] L.Y.M. Gicquel, P. Givi, F.A. Jaber, S.B. Pope, *Phys. Fluids* 14 (2002) 1196–1213.
- [11] K.S. Venkataramani, N.K. Tutu, R. Chevray, *Phys. Fluids* 18 (1975) 1413–1420.
- [12] H. Zhang, C. Tong, *Phys. Fluids* 15 (2003) 1676–1686.
- [13] V. Eswaran, S.B. Pope, *Phys. Fluids* 31 (1988) 506–520.
- [14] M.R. Overholt, S.B. Pope, *Phys. Fluids* 8 (1996) 3128–3148.
- [15] S.B. Pope, *J. Fluid Mech.* 359 (1998) 299–312.
- [16] R.W. Schefer, R.W. Dibble, *AIAA J.* 39 (2001) 64–72.
- [17] C. Tong, J.C. Wyngaard, S. Khanna, J.G. Brasseur, *J. Atmos. Sci.* 55 (1998) 3114–3126.
- [18] C. Tong, J.C. Wyngaard, J.G. Brasseur, *J. Atmos. Sci.* 56 (1999) 2277–2292.
- [19] A.G. Rajagopalan, C. Tong, *Phys. Fluids* 15 (2003) 227–244.
- [20] L.W.B. Browne, R.A. Antonia, L.P. Chua, *Exp. Fluids* 7 (1989) 201–208.
- [21] N. Peters, *Prog. Eng. Combust. Sci.* 10 (1984) 319–399.
- [22] R.S. Miller, S.H. Frankel, C.K. Madnia, P. Givi, *Combust. Sci. Technol.* 91 (1993) 21–52.
- [23] C.D. Pierce, P. Moin, *Phys. Fluids* 10 (1998) 3041–3044.